remote sensing

MDPI

Article

Development and Implementation of an Electronic Crosstalk Correction for Bands 27–30 in Terra MODIS Collection 6

Truman Wilson [1,*], Aisheng Wu [1], Ashish Shrestha [1], Xu Geng [1], Zhipeng Wang [1], Chris Moeller [2], Richard Frey [2] and Xiaoxiong Xiong [3]

1 Science Systems and Applications Inc., Lanham, MD 20706, USA; aisheng.wu@ssaihq.com (A.W.); ashish.shrestha@ssaihq.com (A.S.); xu.geng@ssaihq.com (X.G.); zhipeng.wang@ssaihq.com (Z.W.)
2 Cooperative Institute for Meteorological Satellite Studies, University of Wisconsin, Madison, WI 53706, USA; chrism@ssec.wisc.edu (C.M.); richard.frey@ssec.wisc.edu (R.F.)
3 Sciences and Exploration Directorate, NASA/GSFC, Greenbelt, MD 20771, USA; xiaoxiong.xiong-1@nasa.gov
* Correspondence: truman.wilson@ssaihq.com; Tel.: +1-301-867-2120

Academic Editors: Dongdong Wang and Prasad S. Thenkabail
Received: 20 April 2017; Accepted: 1 June 2017; Published: 6 June 2017

Abstract: The photovoltaic bands on the long-wave infrared focal plane assembly of Terra MODIS, bands 27–30, have suffered from steadily increasing contamination from electronic crosstalk as the mission has progressed. This contamination has a great impact on MODIS data products, including image striping and radiometric bias in the Level-1B calibrated radiance product, and incorrect retrieval in atmospheric products that rely on data from bands 27–30, such as the cloud mask and cloud particle phase products. In this work, we describe the development of an electronic crosstalk correction for bands 27–30 of Terra MODIS using observations of the Moon. In this approach, the derived correction coefficients account for both the "in-band" and "out-of-band" contribution to the signal contamination, which is not considered in previous implementations of the lunar-based correction. The correction coefficients are applied to both the on-board calibrator data and the Earth-view data, resulting in a significant reduction in the image striping and radiometric bias in the Level-1B data, as well as a better performance in the Level-2 cloud mask and cloud particle phase products. This approach will be implemented for Terra MODIS Collection 6 in 2017.

Keywords: MODIS; crosstalk; radiometric improvements; calibration; contamination; cloud mask

1. Introduction

The Moderate Resolution Imaging Spectroradiometer (MODIS) on board the Terra spacecraft is one of the key instruments of the NASA Earth Observing System (EOS) [1]. MODIS is a cross-track, whisk-broom, scanning radiometer, and produces images of the Earth in 36 spectral bands ranging in wavelength from 0.4 μm to 14.2 μm [2]. The MODIS bands are catagorized into two groups based on wavelength, the Reflective Solar Bands (RSB) (<2.1 μm) and the Thermal Emissive Bands (TEB) (>3.6 μm). These bands consist of linear arrays of detectors that are separated onto four focal plane assemblies (FPA) for the visible (VIS), near-infrared (NIR), short- and mid-wave infrared (SMIR), and long-wave infrared (LWIR) bands. As the scan-mirror rotates, an image is projected onto the FPAs and is sampled by the detectors at a rate that coincides with the scan-mirror rotation rate, producing a continuous image. In addition to Earth-view imagery, the scan-mirror also brings into view a set of on-board calibrators (OBC) and deep-space during each scan-mirror rotation, which is able to provide calibration data for the instrument on-orbit and the background signal respectively. Each of the bands

is calibrated on-orbit using these OBCs, which include the solar diffuser (SD) with its associated SD stability monitor (SDSM) for calibrating the RSBs [3], the blackbody target (BB) for calibrating the TEBs [4], and the spectroradiometric calibration assembly (SRCA), which is used for spatial and spectral characterization of the MODIS detectors [5]. MODIS also uses observations of the Moon through the space-view port [6] and Earth-view targets [7,8] in order to determine the degradation of the scan mirror response as a function of angle of incidence on the scan mirror.

The LWIR bands, 27–36, are located on a cold focal plane, which has a controlled temperature at 83 K, and consist of bands using both photovoltaic (PV) detectors (27–30) and photoconductive (PC) detectors (31–36). The LWIR PV bands are used to measure water vapor distribution, cloud properties, and ozone concentrations, and range in center wavelength between 6.7 μm and 9.7 μm. These bands also share the same sampling electronics used for readout of the detector signals, and are sampled in succession for each MODIS pixel. The use of shared sampling electronics gives rise to the potential for electronic crosstalk between the detectors of the LWIR PV bands. This has been an issue that has been monitored since before the launch of the Terra spacecraft. As the mission has progressed, the effects of electronic crosstalk among the LWIR PV bands have become apparent through sudden gain changes of the detectors, increases in the noise-equivalent difference temperature (NEdT) [9], striping in the images, and the presence of land/water boundary features in atmospheric channels that did not observe these features early in the mission [10–14]. These effects have a great impact on MODIS data products that use bands 27–30 [14].

Electronic crosstalk is a problem that occurs in many space-based imaging instruments [15–17]. In the case of Sentinel-2, the crosstalk contamination was characterized using ground-based measurements before launch [15]. By directly illuminating individual bands on the instrument, the impact of electronic crosstalk can be measured on each of the affected bands, and correction coefficients can be derived to use during the mission. Similar measurements were performed during the prelaunch phase for MODIS which found that there was crosstalk present in many MODIS bands, although at a relatively low level. However, significant on-orbit changes preclude us from being able to use these characterizations for correcting the MODIS data for the LWIR PV bands. Other spaced-based missions, such as CERES [16] and MOST [17], use noise-based characterizations to provide corrections to the electronic crosstalk contamination. Optical crosstalk can also be an issue in missions such as ASTER [18] and also for the PC bands in MODIS [4], and have been corrected using analysis of Earth-view imagery and observations of the Moon respectively. While some signs of optical crosstalk contamination exist for the LWIR PV bands in Terra MODIS, these features are small, especially when compared to the electronic component of the contamination.

For electronic crosstalk in both Aqua and Terra MODIS, observations of the Moon through the space-view port have been used extensively to characterize the crosstalk contamination [10–14,19,20]. For both instruments, signal contamination in the lunar images is clearly observed for bands 5–7 and bands 20–30. For most of these bands, the impact on the Level-1B data is small. However, for the LWIR PV bands in Terra MODIS, the contamination levels have increased greatly as the mission has progressed, including a large increase during the Terra MODIS safe-mode event in February of 2016 [14]. While the increase from the safe-mode event may be caused by thermal stresses introduced to the electronics during the warm-up and cool-down of the cold FPA, the reason for the much greater impact from electronic crosstalk on the LWIR PV bands in Terra MODIS remains unknown. For Aqua MODIS, the instrument and electronics are nominally identical, and even though electronic crosstalk is observed for the LWIR PV bands in Aqua MODIS [20], the impact on the Level-1B data is much lower than what is seen for Terra and the contamination level changes significantly less over time, even though both instruments have been in operation for more than 15 years.

To characterize and correct the signal contamination from electronic crosstalk in this work, we also use observations of the Moon through the MODIS space-view port to derive the appropriate correction coefficients that can be applied to the data from bands 27–30. Unlike previous work done for the LWIR PV bands in MODIS [10–13], we consider the contribution to the crosstalk signal from detectors

within the same band as the contaminated detectors as well as the out-of-band signal. The in-band contribution has a particularly large impact on the correction to band 29, where the in-band contribution to the crosstalk is greatest [14]. The method for correcting the crosstalk effect is based on a linear model, similar to previous works [10–13], where the correction signal is linearly proportional to the measured signal from the detectors sending the contamination. The derived coefficients are applied to MODIS Level-1A data, from which the higher level data products can be derived and evaluated.

In this work, we also discuss properties of the derived coefficients and identify the cause of the sudden increase in the contamination levels throughout the mission. The derived coefficients are then applied to both the OBC data to correct the gain coefficients and to the Earth-view images. We then discuss the impact of the correction on MODIS Level-1B data and MODIS Level-2 atmospheric products. Overall, the crosstalk correction provides a significant improvement to the MODIS Level-1B and Level-2 data. This correction will be implemented in Terra MODIS Collection 6 forward processing starting in July 2017, along with a reprocessing of the entire mission's data record.

2. Characterization of the Crosstalk Effect

To develop a correction to the crosstalk contamination in the LWIR PV bands, it is important to first understand what effect the contamination has on the MODIS data. The contamination occurs at the earliest stages of the electronic readout from the detectors, and affects the raw digital signal output of the instrument. This means that the contamination will affect the data at every level, starting with the derivation of the gain coefficients from the OBC data and the raw Earth-view data, with cascading impacts to higher level products that use data from the LWIR PV bands.

Over the course of the Terra mission, contamination of the LWIR PV bands in MODIS has steadily increased, and has resulted in increasingly poor image quality and a drift in the brightness temperature retrieval relative to other bands. For band 27, the impact has been particularly large, as seen in Figure 1. In this figure, we show images from band 27 over the Great Lakes region in North America at times with relatively few clouds in the scene. Since band 27 is a channel used primarily to measure water vapor in the atmosphere, it is not expected to be able to distinguish between land and water surfaces in the retrieved images. Early in the mission (Figure 1, left), when there is little contamination, this is the case. However, as the mission progresses, the boundary between land and water begins to appear more distinctly (Figure 1, center and right). These features are a strong indication of electronic crosstalk among the LWIR PV bands, as images from bands 29 and 30 show these features clearly. Also, using geolocation data from the MOD03 data product shows that the land/water boundary is offset by several pixels in the scan direction from its nominal location. This is consistent with the contamination features being caused by electronic crosstalk because of the spatial offset of bands 29 and 30 relative to band 27 on the FPA.

In the lower part of Figure 1, we show histograms for the brightness temperature retrieval for the granules containing each of the images for each detector in band 27. For the data in 2000, each detector has a similar retrieval in brightness temperature over the granule, which is expected for well calibrated data over a large scene. In 2008, the contamination has increased, leading to detector-to-detector differences in the brightness temperature profiles. These detector-to-detector differences manifest themselves as striping in the band 27 images. By 2016, the contamination has increased significantly, and the brightness temperature retrieval among the detectors varies dramatically. The image for 2016 shows significant striping and land feature contamination. This increase in the crosstalk contamination in 2016 was caused by the Terra MODIS safe-mode event which occurred on 18 February 2016 [14]. This event caused a significant increase in the crosstalk contamination for nearly every detector in bands 27–30.

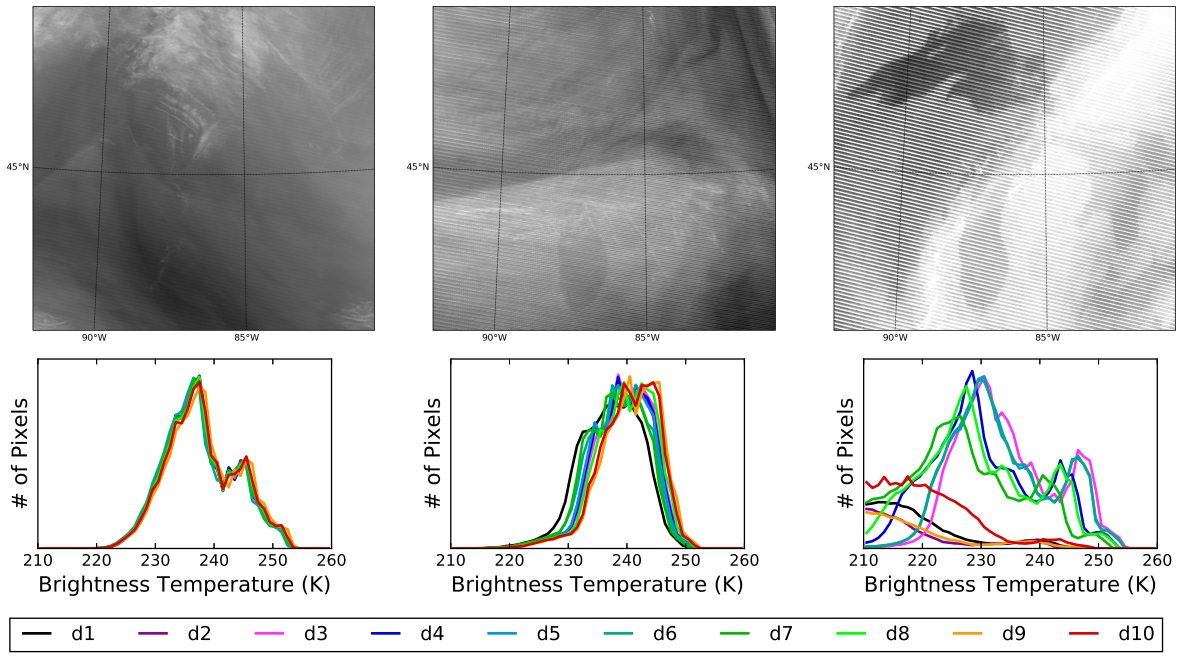

Figure 1. (top) Example images showing the increase in contamination from electronic crosstalk in Terra MODIS band 27 over the Great Lakes region on 3 May 2000; 4 May 2008; and 22 May 2016 from left to right. (bottom) Histograms for the entire 5 min granule that contains each of the above images showing the brightness temperature retrieval for each detector within band 27. In 2016, the spread in brightness temperature for detectors 1, 2, 9, and 10 is extreme, and extends beyond the left edge of the plot. The full histogram can be seen in Figure 10.

The crosstalk contamination can also be seen in observations of the Moon through the MODIS space-view port, where the dark background of space surrounding the bright lunar image shows contamination features clearly. Since the angular size of the Moon is small at the relatively large distance between the spacecraft and the Moon, the image of the Moon on the MODIS FPA does not illuminate all bands and detectors simultaneously, as seen in Figure 2a. Also, due to the oversampling effect [6], the Moon can be observed over the course of many consecutive scans, with the lunar image moving in the track direction by less than the width of a single MODIS 1-km pixel from scan-to-scan.

For each MODIS detector within a given band, the lunar signal can be plotted versus scan and frame number as seen in Figure 2b, creating an effective single detector lunar image. At the highest signal levels, the lunar signal saturates during analog-to-digital conversion at a maximum signal of 4095 before background subtraction (Figure 2b is shown after background subtraction). For each scan, the background signal level is determined using the average signal of 6 frames on each side of the main lunar signal (12 total), which begin 15 frames away from the center frame for the lunar observation. The center frame is calculated for each band and lunar event based on the known orientation of the instrument after the roll maneuver and the position of the moon relative to the instrument.

Since the electronic crosstalk occurs at the earliest stages of the detector electronics before the analog-to-digital conversion of the signal, this saturation needs to be corrected in order to have a better representation of the true contaminating signal. To do this, we use the ratio of the unsaturated pixels with the spatially co-registered (aligned in frame number) signal from band 31, which does not saturate when viewing the Moon. We then multiply the band 31 signal by this ratio to replace the values of the saturated pixels.

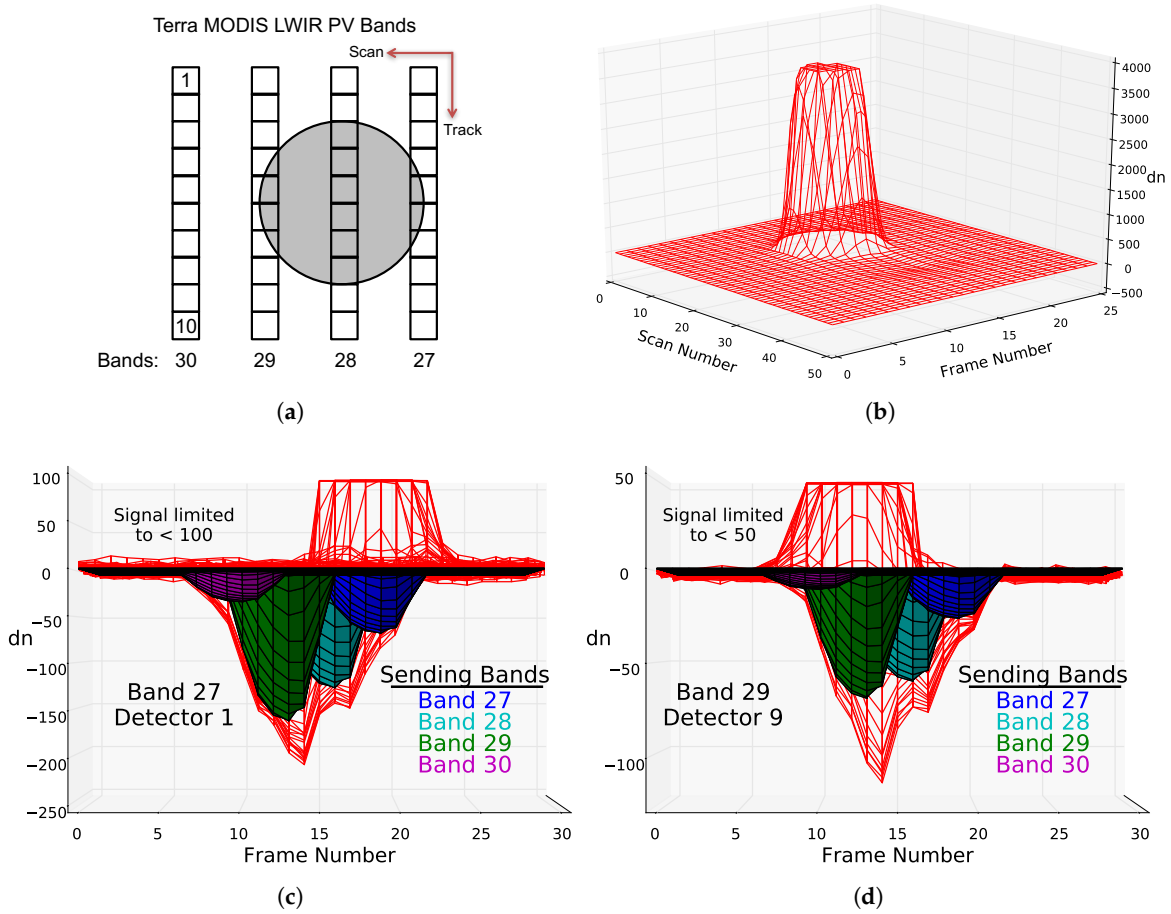

Figure 2. Example signals from lunar images from the LWIR PV bands. In (**a**), we show the layout of the LWIR PV bands on the FPA, with a circle superimposed representing the relative size of the lunar image on the FPA. The detectors are labeled in product order. In (**b**), we plot the background-subtracted signal versus scan and frame number for a single detector (Band 29, Detector 9). The peak of the signal saturates when viewing the moon because of the high brightness temperature relative to the usual Earth-view scene data. In (**c**,**d**), we show the lunar signal limited to low signal levels, where the negative signal is due to crosstalk contamination. On these plots, we also show the alignment of the sending band signals, which are derived from the measured lunar signal of the sending bands. The sending signals are shown after a saturation correction has been applied, and are scaled to show alignment. In (**b**–**d**), the data is from a lunar observation on 19 February 2014. (**a**) LWIR PV Bands; (**b**) Single Detector Lunar Signal; (**c**) Band 27 Signal Alignment; (**d**) Band 29 Signal Alignment.

At the lowest signal levels, just around the main lunar signal, contamination of the lunar images can be seen in the form of a negative signal level ($dn < 0$), meaning the signal measured is below the background level, as seen in Figure 2c,d. To determine the source of the contaminating signal, we can use the known frame offsets between each LWIR PV band (3 frames between each band), and plot the scaled lunar signal from each band versus the contamination. In Figure 2c,d, we see that all of the LWIR PV bands, 27–30, are sending a contaminating signal, including signal that is sent from other detectors within the same band. This in-band correction is not considered in previous correction attempts using the moon [10–13], and has a particularly large impact on the correction results for band 29 [14]. Since there are only 3 frames of separation between each of the LWIR PV bands on the FPA, there is significant overlap between lunar signals observed by each of the bands when plotted versus the frame number. We observe that the small peaks in the total contamination signal occur in between the peaks of the individual sending signals due to this signal overlap.

The Moon provides a good source not only for identifying the contaminating signal, but also for deriving the appropriate correction coefficients, as the contamination occurs near where the signal is close to the background level. This allows us to make a comparison to the expected "true" signal, which becomes difficult if analyzed using data from Earth-view scenes. In the next section, we describe the development of an algorithm using scheduled lunar observations to derive correction coefficients throughout the mission.

3. Algorithm

The lunar images that we used to identify the contaminating signal can also be used to develop an algorithm for deriving correction coefficients, which can then be applied to correct the Earth-view images. Similar to previous works [10–13], the crosstalk contamination signal is assumed to be linearly proportional to the signal from each of the sending detectors as seen in Equation (1), where the corrected digital signal is defined as:

$$dn_i(S,F) = dn_i^*(S,F) - \sum_j c_{i,j} \cdot dn_j^*(S,F+\Delta F_j) \quad (1)$$

Here, dn_i^* is the measured (contaminated) background subtracted digital signal from the ith LWIR PV detector, and S and F represent the scan and frame number of the measurement respectively. The summation term represents the contaminated signal, which when subtracted from the measured signal gives the corrected signal, dn_i. Inside the summation, $c_{i,j}$ is the crosstalk coefficient matrix which scales the signal from the jth LWIR PV detector to represent the contamination, and ΔF_j is the appropriate frame offset of the sending band relative to the receiving band on the FPA. In this equation, i and j range from 1–40 to represent detectors 1–10 of bands 27–30 in product order, and $c_{i,j} = 0$ when $i = j$.

To calculate the elements of $c_{i,j}$, we first need to compare the contaminated signal for each detector to a reference signal, which we can take to be an approximation of the uncontaminated data. While fitting the corrected signal to a "flat" background level for pixels just outside the main lunar signal seems like a reasonable approach, we found that for many bands that have a high signal level when observing the moon, such as bands 13, 14 (high gain), 31, and 32, there is a slow roll-off in the lunar signal near the background level, particularly in the track direction. These bands have no clear signs of electronic crosstalk contamination like that of bands 27–30, so it is unlikely that this low-signal behavior is related. We found that when using a reference signal for fitting the coefficients, the quality of the correction to the lunar data improved greatly.

For this work, we used band 31 as our reference signal. For this reference signal, we accounted for the expected difference in the low-signal behavior, which is primarily due to the lower gain of band 31. The gain difference is corrected by multiplying the band 31 signal by the ratio of the sum of unsaturated pixels of our receiving detector and the spatially co-registered detector of band 31, much like the saturation correction was applied previously. To account for additional minor differences in the shape of the reference signal, we compared our measured signal to the gain-corrected reference signal for lunar observations early in the mission when the magnitude of the crosstalk contamination is negligible. By deriving crosstalk coefficients for this early mission data, we determined the bias in the coefficient values that are associated with these small shape differences. We can then use these coefficient values as a zero-point reference for the coefficients throughout the mission.

We take the difference between our reference signal and measured signal to be the amount of contamination for each detector. We then use a least squares fit to find the values for the elements of $c_{i,j}$ that minimize the value of η_i^2 in Equation (2) for the ith detector.

$$\eta_i^2 = \sum_{S,F} \left(dn_i^*(S,F) - dn_{ref,i}(S,F) - \sum_j c_{i,j} \cdot dn_j^*(S,F+\Delta F_j) \right)^2 \quad (2)$$

In this sum, the scans/frames used do not include signal from the main lunar peak of the ith detector, as the large signal measured when viewing the moon can obscure the contamination. In this work, we define pixels to be part of the main lunar signal if the background subtracted digital count is greater than 150 for the band 31 reference signal.

While this algorithm is able to find values for each of the elements of $c_{i,j}$ individually, in practice, we found that significant overlap in the sending signal among neighboring detectors within a band made a truly independent determination of the individual coefficients difficult. To circumvent this issue, we imposed a restriction for each coefficient value to be the same for each sending detector within a given band, producing an effectively band-averaged result, similar to previous works [10–13]. However, there are a few important exceptions. These exceptions take into account the anomalous sending signal from detector 10 of bands 27, 28, and 29 to detector 1 of bands 28, 29, and 30 respectively. In these cases, a separate sending signal can be seen in the lunar images for detector 1 of bands 28–30 that is precisely aligned with the lunar signal from detector 10 of bands 27–29, as described in [14]. The coefficient for these sending detectors is found independently of the band-averaged coefficient results, and improves the performance of those contaminated detectors. This contamination effect is likely due to an electronic sampling error when the electronics used to read the detector signals switch between neighboring bands. A similar effect was observed and corrected in Aqua MODIS band 24 using lunar images, and further investigations into this effect are on-going [19].

After solving for the coefficient values, we can perform an initial test of the effectiveness of the correction coefficients by applying them to the lunar data and comparing to the original contaminated signal, as seen in Figure 3. In this figure, the red data shows the lunar signal before the correction is applied, and the black data represents the corrected signal using our derived coefficients. From this, we can see that the large negative signal from the contamination is removed entirely, including the component from within the same band as the contaminated detector. Similar results are seen for each detector in the LWIR PV bands.

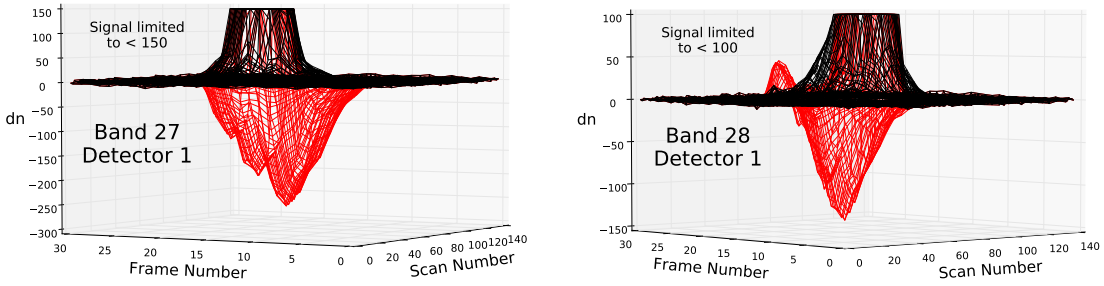

Figure 3. Example corrections for lunar data from 4 August 2015. The red data is before correction and the black data is after correction.

In the right plot of Figure 3, we show the results for band 28, detector 1, where there is an anomalous sending signal from band 27 detector 10, seen as the positive peak away from the main lunar signal. By solving for this sending coefficient separate from the rest of the band, we are able to correct this positive contamination signal as well as the negative contamination signal sent from the rest of the band simultaneously. The changes seen in this separate coefficient throughout the mission are similar to those seen for the coefficients within the rest of the band with an added offset. This contamination occurs throughout the entire mission for detector 1 of bands 28–30.

The algorithm for determining the crosstalk coefficients is simple and robust, and can be used for each lunar observation by the instrument in order to determine the crosstalk coefficients. In our current implementation (Section 4.3), the coefficients are derived only from scheduled lunar observations, where the lunar phase angle is restricted to be within a specified range [6]. In the future, it may be beneficial to use unscheduled observations, where the moon appears in the space-view port without any spacecraft maneuvers, for validation purposes. These unscheduled observations may occur over

many consecutive orbits over a large phase angle range. At large lunar phase angles, there may be an added benefit of having less saturation for the MODIS TEBs. However, since no spacecraft maneuvers are performed, these observations do not always provide a complete lunar image through the space-view port.

4. Crosstalk Coefficients and Gain Correction

Using the algorithm described in Section 3, we derived crosstalk correction coefficients for each detector of each LWIR PV band using every scheduled lunar observation (∼monthly) throughout the mission. An example of the trending coefficients for one detector from each band can be seen in Figure 4. The coefficient values for every detector show both a slow increase in magnitude throughout the mission as well as occasional sudden increases in the values of the coefficients. In general, the values of the coefficients for each contaminated detector trend towards increasingly negative values as the mission progresses.

While the crosstalk coefficients were derived independently for each contaminated detector in the LWIR PV bands, the relative values of the coefficients from each sending band are similar for every contaminated detector. For instance, the magnitude of the crosstalk coefficients are largest for sending band 29, followed by sending bands 28, 27, and 30 respectively. An example of this relationship is seen in Figure 4, however, it is a characteristic for every contaminated detector in the LWIR PV bands throughout the entire mission, regardless of the time-dependence or the overall scaling of the contamination.

To characterize this relationship, we evaluated the relative magnitudes of the coefficients from each sending band for every detector throughout the entire mission, excluding the detector 10 to detector 1 contamination coefficient discussed previously. For a given detector, we can plot the time-dependent coefficients using the following equation:

$$y\left(c_{i,B}(t)\right) = \frac{c_{i,B}(t)}{c_{i,B_{29}}(t)} \cdot c_{i,B}(t) \tag{3}$$

where $c_{i,B}$ is the crosstalk coefficient for the ith contaminated detector from sending band, B (27–30). If we plot Equation (3) using the values of $c_{i,B}(t)$ on the x-axis, the slope of a linear fit to the data is the relative magnitude of the crosstalk coefficient with respect to the coefficient from band 29, represented by the term $c_{i,B}(t)/c_{i,B_{29}}(t)$. An example of these plots can be seen in the top row of Figure 5 with their associated fit lines.

For each contaminated detector, we can calculate the best fit value for the slope of Equation (3) for coefficients from each sending band. Since we are comparing each coefficient to the values from band 29, the slope of the band 29 coefficients will be unity by definition. However, the slope found for each of the other bands represents the relative magnitude of the coefficients in relation to band 29. In the lower part of Figure 5, we plot the calculated slope for each sending band for every LWIR PV detector. As seen previously, the largest coefficients are from sending band 29, followed by 28, 27, and 30 for every contaminated detector. In addition, it also appears that the relative magnitudes of the coefficients between the bands remains at nearly the same level for every detector in the LWIR PV bands, even though the absolute magnitude of the coefficients for each detector changes throughout the mission independently.

This property of the contamination could be beneficial for derivations of the crosstalk coefficients from other sources with a higher frequency of observations than the Moon. Such a property would impose a fixed relationship between the sending band coefficients, including the in-band contribution, that would reduce the number of unknown parameters for each contaminated detector to a single coefficient.

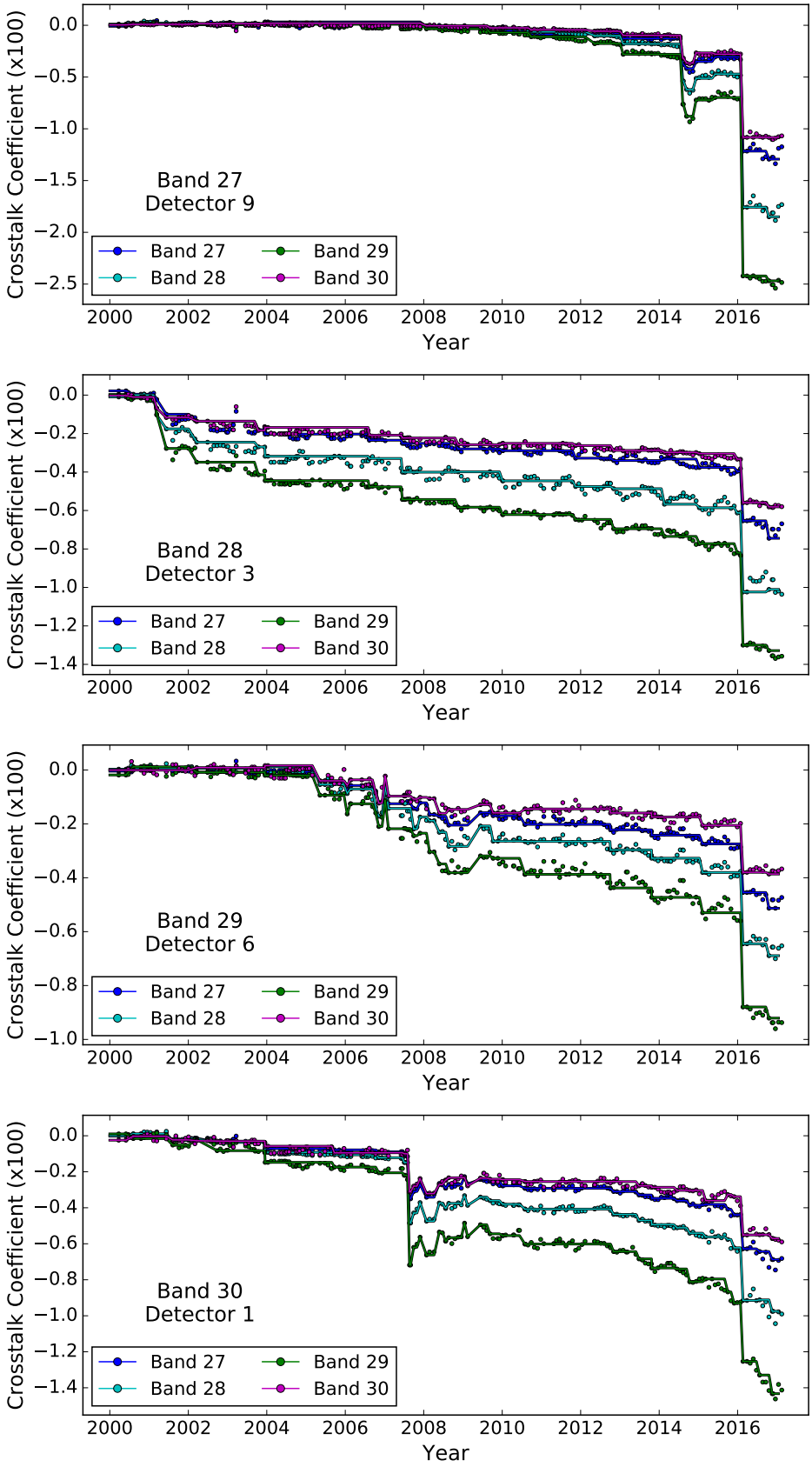

Figure 4. Example of the trending coefficient values derived from lunar observations. The circles represent the coefficients derived from individual lunar observations. The lines show the coefficient values used in Collection 6, based on the criteria described in Section 4.3.

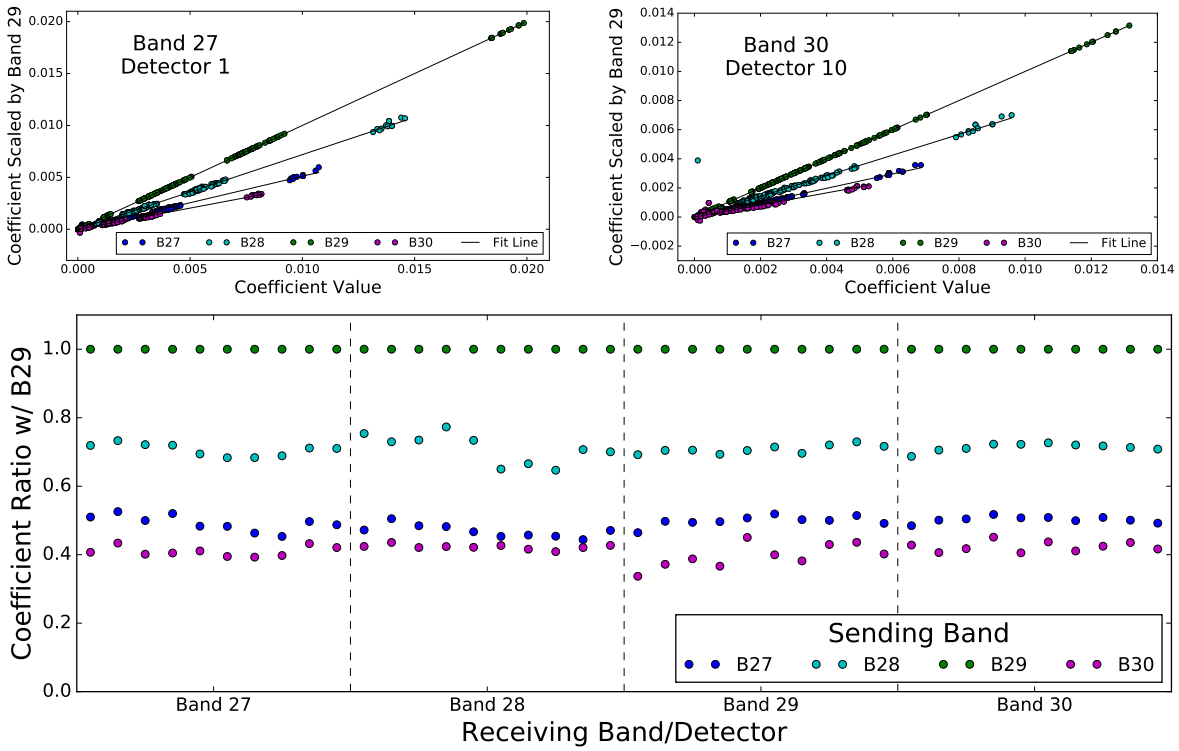

Figure 5. Comparison of the correction coefficient values for each contaminated detector. In the top two figures, the coefficient values (x-axis) are plotted against the coefficient values squared divided by the band 29 sending coefficient (y-axis). Here, the slope of the fitted line represents the relative magnitude of the coefficient compared to the band 29 sending coefficient for the entire dataset. In the lower figure, we plot this relative magnitude for each band/detector in the LWIR PV bands. By definition, the band 29 coefficient ratio is equal to 1.

4.1. Gain Correction

The crosstalk contamination occurs at the earliest stages of the electronics, and therefore affects all of the data that is derived from the raw signal output, including the derivation of the detector gain coefficients. Accurate determination of the instrument gain coefficients is vital for producing climate quality measurements of the Earth-view scene radiance, and any significant bias in the gain values will have an impact on the downstream Level-1B and Level-2 products. The Level-1B Earth-view scene radiance is given by Equation (4).

$$L_{EV} = \frac{1}{\mathrm{RVS}_{EV}} \left(a_0 + b_1 dn_{EV} + a_2 dn_{EV}^2 - (\mathrm{RVS}_{SV} - \mathrm{RVS}_{EV})\, L_{SM} \right) \tag{4}$$

Here, a_0, b_1, and a_2 are the offset, linear, and quadratic gain coefficients respectively, dn_{EV} is the background-subtracted digital counts of the Earth-view scene, RVS is the response versus scan angle of the scan mirror (the subscripts EV and SV represent the Earth-view and space-view ports respectively), and L_{SM} is the background radiance of the scan mirror. The linear gain coefficient, b_1, is determined on-orbit on a scan-by-scan basis using the BB calibration source at a fixed temperature [4,9]. The non-linear coefficients, a_0 and a_2, are determined during regularly scheduled BB warm-up/cool-down calibration events, where the BB temperature is cycled away from its nominal set-point in order to assess the non-linear response of the detector as a function of BB temperature. However, in Collection 6, the offset term a_0 is fixed to a value of zero for mirror-side one.

The crosstalk contamination greatly affects the determination of the gain coefficients as seen in Figure 6, where plots of the uncorrected and corrected linear gain coefficients are shown for each

band. Before correction, the crosstalk contamination introduces large drifts and sudden changes to the gain coefficients over time, as well as an increased spread in the gain values from detector-to-detector within a band. After correction, these drifts in the gain are reduced significantly, particularly after the safe-mode event in early 2016. The non-linear coefficients, a_0 and a_2, are also affected by crosstalk contamination, particularly for band 27, detectors 1, 2, 9, and 10 and band 30 detector 8 [13,14] after the safe-mode event. To reduce the impact of these effects, a_0, b_1, and a_2 are corrected for all LWIR PV bands and detectors in the MODIS Level-1B data. These corrections provide a significant improvement to both the Level-1B calibrated images as well as downstream science products, as discussed in Sections 5 and 6.

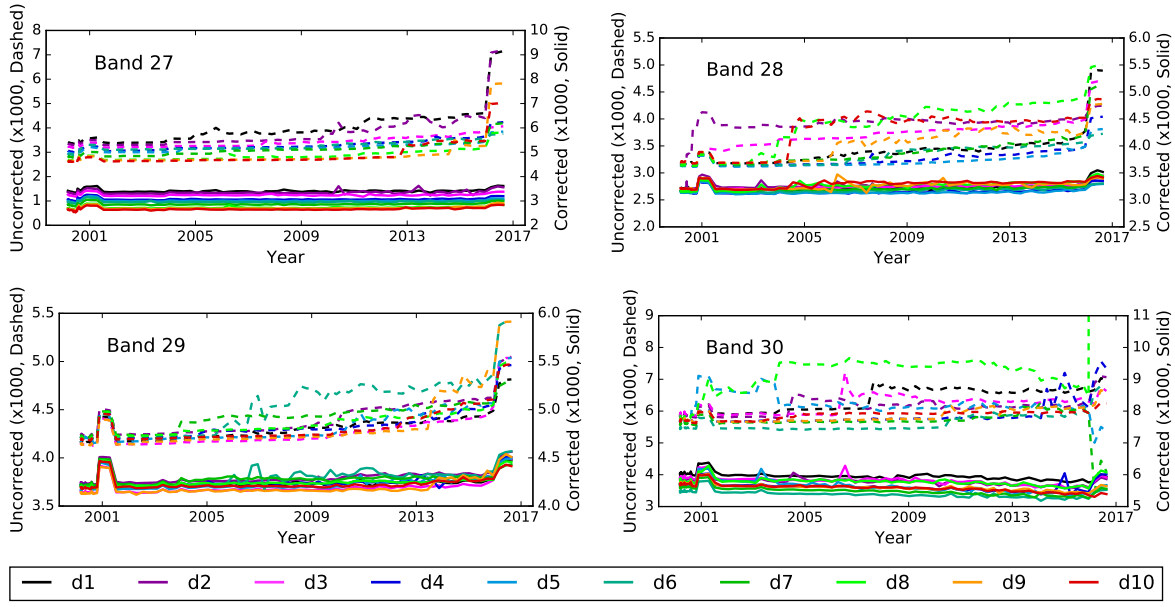

Figure 6. Plots of the linear gain coefficient, b_1, before (dashed) and after (solid) application of the crosstalk correction, taken from BB warm-up/cool-down data throughout the Terra MODIS mission. For clarity, separate scales are used for the uncorrected (**left**) and corrected (**right**) data, where the overall scale is shifted, but kept at a fixed range, to allow for comparison between the uncorrected and corrected data while preventing significant overlap in the data. For band 30, the scale is truncated because of the extreme change in the gain coefficient for detector 8 for the uncorrected data.

4.2. Characterization of the Coefficient Jumps

Over the course of the Terra mission, the crosstalk contamination for each of the LWIR PV bands has increased steadily. However, as seen in Figure 4, there have also been anomalous events where the crosstalk contamination increases suddenly between the lunar observations that we use to determine the crosstalk coefficient values. Outside of the Terra safe-mode event [14], typically only a single detector is affected by each event. To better understand this phenomena, it is necessary to evaluate the relationship between the crosstalk contamination and the derived detector gain on-orbit.

For MODIS TEB, the linear gain parameter, b_1, is derived on-orbit on a scan-by-scan basis, as the rotating scan-mirror brings the BB source into view of the detectors each scan. For most bands among the TEB, b_1 changes slowly on-orbit [4,9]. However, for the LWIR PV bands, the crosstalk contamination has a significant impact on the derived gain, leading to relatively large changes throughout the mission, as seen in the left plot of Figure 7, where b_1 is derived for a single granule for each day throughout the mission. When the crosstalk coefficients are plotted with the gain parameter b_1, it is clear that there is a correlation between increases in the derived crosstalk coefficients and increases in b_1. Therefore, we can use the derived value of b_1 to determine the time at which the sudden changes in the crosstalk contamination occur.

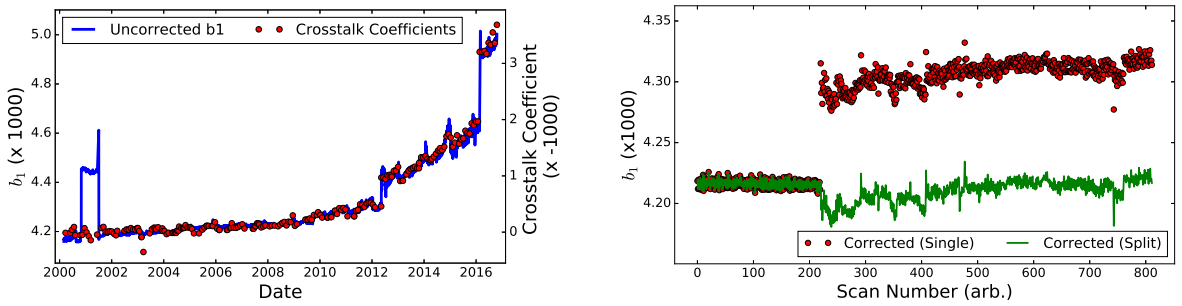

Figure 7. Example of the change in the value of b_1 for band 29, detector 10 in Terra MODIS over the whole mission (**left**) and over a short time period on 11 May 2012 (**right**). In the left figure, we also plot a scaled version of the crosstalk coefficients (right axis) over the values of b_1. Early in the mission ($\sim$2001), the change in b_1 is related to the change the electronics side from side-A to side-B and then back, and is unrelated to the crosstalk issue. In the right figure, we show the crosstalk correction on the scan-by-scan b_1 using a single set of correction coefficients (red), and using the correction coefficients derived from surrounding lunar events, split about the scan where there is a jump in the value of b_1 (green).

To find the timing of these sudden changes, we first determine the date of the event using the values of b_1 from each day of the mission. We then evaluate the scan-by-scan b_1 values for each granule from the chosen day and search for sustained changes in the value of b_1, an example of which can be seen in the red data of the right plot of Figure 7. By determining the precise scan number where the increase in the crosstalk contamination takes place, we are able to accurately determine the location of the satellite relative to the Earth's surface during these events. As of this writing, we have detected 41 separate events. The geolocation of each event can be seen in Figure 8. For the majority of the events, the spacecraft was located in the South Atlantic Anomaly (SAA), where the Earth's magnetic field strength is relatively weakened. In this region, there is a higher flux of high-energy charged particles which have been known to cause damage in spacecraft electronics [21], and appears to be the main contributor to the sudden increases in the crosstalk contamination for the LWIR PV bands throughout the mission.

When applying the crosstalk correction throughout the mission, it is important to account for these sudden changes in the level of contamination. Since we have a limited number of lunar observations, the most appropriate way to account for these events is to use the correction coefficients from the preceding lunar observation before the event, and from the following lunar observation afterwards. By doing this, we can produce more consistent values of the gain coefficient across the event, as seen in the green data of the right plot of Figure 7. In this example, the scan-by-scan gain is successfully corrected using two sets of coefficients from lunar observations. However, in many cases the sudden change in the gain can take many minutes and even days to settle after the anomalous event occurs. In the future, a method for deriving crosstalk coefficients at a higher frequency may be desired, as mentioned previously, in order to provide a better correction for gain changes in between lunar observations.

Since the crosstalk coefficients cannot be changed in the middle of a data granule, we handle these data jumps by creating a new set of correction coefficients with a time-stamp immediately following the granule with the data jump. For this time-stamp, detectors with a significant gain change use the derived coefficient values from the next lunar observation, with all the other detectors using the coefficient values from the preceding lunar observation. For forward processing, this type of correction becomes difficult because the future lunar observations will be unavailable. However, since the data jumps typically only affect a single detector, the impact of missing data jumps should be minimal.

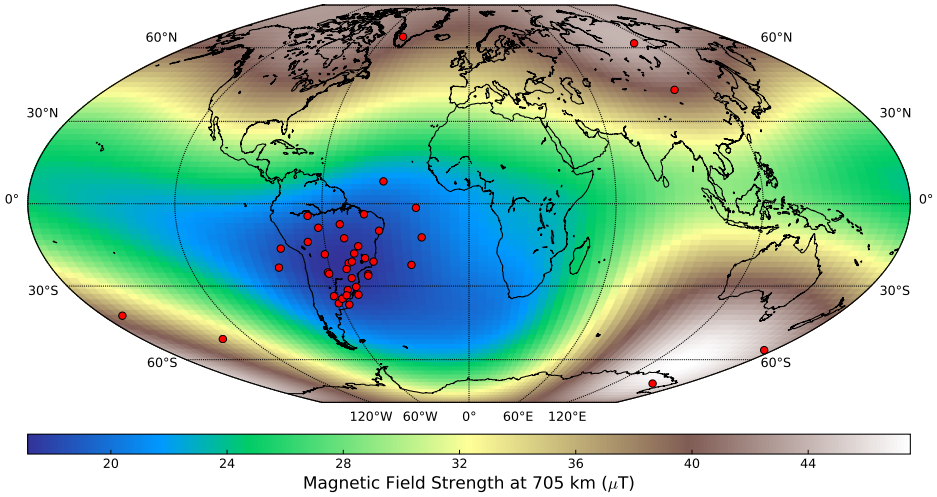

Figure 8. A map of the geolocation of the instrument (red dots) for each significant change in the crosstalk coefficients as determined by the scan-by-scan gain change on-orbit (Figure 7). The colormap shows the magnetic field strength at the nominal altitude of the Terra spacecraft (705 km) in μT. Most of the events occur in the South-Atlantic Anomaly, which is a region of relatively low magnetic field strength.

4.3. Determining the Collection 6 Coefficient Values

For implementation in Collection 6, we do not use the coefficient values derived from every scheduled lunar observation. Instead, for each detector, we evaluate the impact of the change in crosstalk coefficients on the linear gain parameter, b_1, for that detector. For each new lunar observation, we calculate the average value and standard deviation of b_1 for an entire days worth of granules (288) both with the previous and new sets of crosstalk coefficients and compare with the value of b_1 from the dates associated with the previous 10 lunar observations. If we detect a change in b_1 that is outside the standard deviation, greater than 0.75% of the value of previous b_1 values, and corrects the value of b_1 to be closer to that of the previous b_1 values, then we update the coefficients for that detector. A comparison of the Collection 6 coefficient values compared to the values derived from each lunar observation can be seen Figure 4.

This method for updating the coefficients reduces the number of updates needed for each detector considerably compared to the total number of lunar observations. Analysis of the L1B data using the Collection 6 coefficients versus the raw coefficient values showed that the differences in the L1B were negligible. This technique for updating the coefficients is applied throughout the entire mission, and will continue during forward processing of Collection 6.

5. Correction of MODIS Level-1B Data

Since the electronic crosstalk among the LWIR PV bands occurs on the raw signal level, its impacts can be seen on every level of MODIS data. For the MODIS Level-1B (L1B) data, which provides the calibrated radiance of the Earth-view scenes, electronic crosstalk has a significant impact on both the derived gain coefficients of the detectors and on the raw Earth-view signal. This leads to a clear degradation of the image quality, as shown in Figure 1.

The radiance for the L1B data product is calculated using Equation (4). With the gain coefficient correction described in Section 4.1, and a crosstalk correction applied to the Earth-view signal, dn_{EV}, the Level-1B calibrated radiance can be re-derived for any data granule throughout the entire mission. Figure 9 shows the crosstalk correction applied to an Earth-view image using band 27 over the Great Lakes region on 22 May 2016. For band 27, the effects of the contamination are the most severe when compared to the other LWIR PV bands, where the crosstalk introduces significant striping due to

detector-to-detector differences in the contamination levels and introduces land/water boundary features to the image, which should not be seen in band 27 images. When the correction is applied, the land/water boundary features are removed almost completely, along with a significant reduction in the image striping.

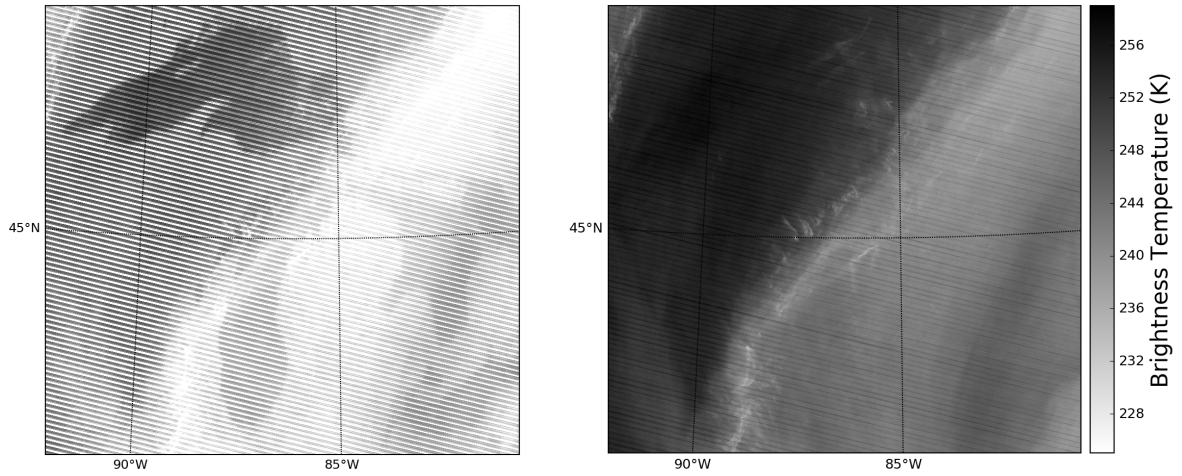

Figure 9. Example image correction for L1B data over the Great Lakes region on 22 May 2016 for Band 27 with the uncorrected image to the left and the corrected image to the right.

In Figure 10, we show histograms of the brightness temperature retrieval for each LWIR PV band over the same scene as Figure 9. Each L1B data granule is comprised of 202−204 scans, each of which contains an image swath of the Earth for each detector of 1354 individual frames. This means that for each granule, each detector has approximately $2.7 \cdot 10^5$ brightness temperature retrievals on the pixel level. For well-calibrated detectors over this many samples, it is expected that a histogram of the brightness temperature retrieval for each detector will be nearly the same. However, for detectors with varying levels of contamination, as is the case of the LWIR PV bands, electronic crosstalk introduces large variations among the detectors in the histograms of the brightness temperature retrievals. The differences are particularly large for band 27, detectors 1, 2, 9, and 10, and band 30, detector 8. After the correction is applied, we see significant reductions in the detector-to-detector differences for every band. This shows that the derived correction coefficients for each contaminated detector produce consistent data over the entire scene, even though the magnitude of the contamination is different for each detector.

To analyze the impact of the correction over the entire mission, we can use data over selected reference sites to monitor the trending of the retrieved brightness temperature relative to band 31, which is considered to be a stable reference band. In Figure 11, we show plots of the brightness temperature drift before and after correction for bands 27, 29, and 30 over the north Atlantic Ocean and for band 29 over Dome C in Antarctica. For the ocean data, we selected scenes with relatively few clouds and an average brightness temperature in band 31 of greater than 270 K over the entire mission. For bands 27 and 29, a measurable change in the relative brightness temperature begins to appear in about 2005, and increases steadily throughout the rest of the mission up to the present. In early 2016, the Terra spacecraft went into safe-mode, and upon recovery, the crosstalk contamination among the LWIR PV bands increased significantly, which can be seen as a sudden change in the brightness temperature drift in the data from the Atlantic Ocean.

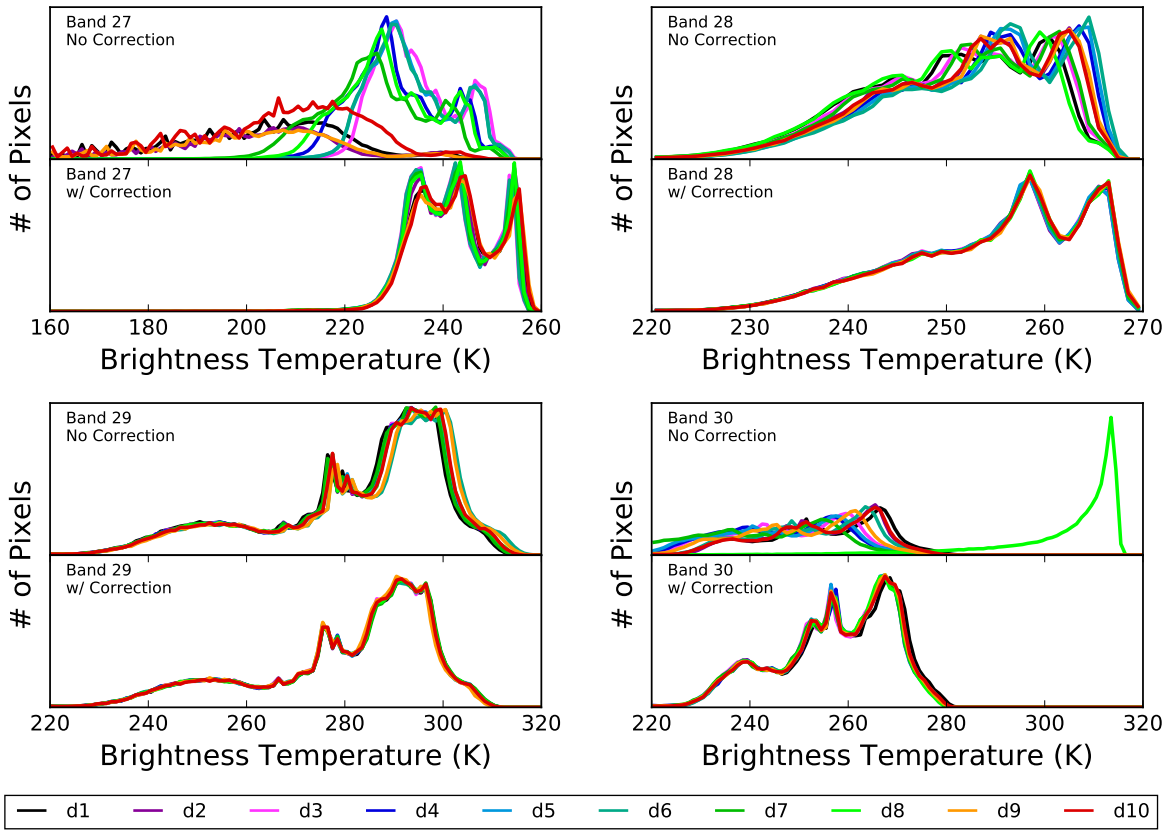

Figure 10. Histograms of the brightness temperature retrieval for the entire granule that contains the image in Figure 9 (2016143.1655) before and after correction for each LWIR PV band.

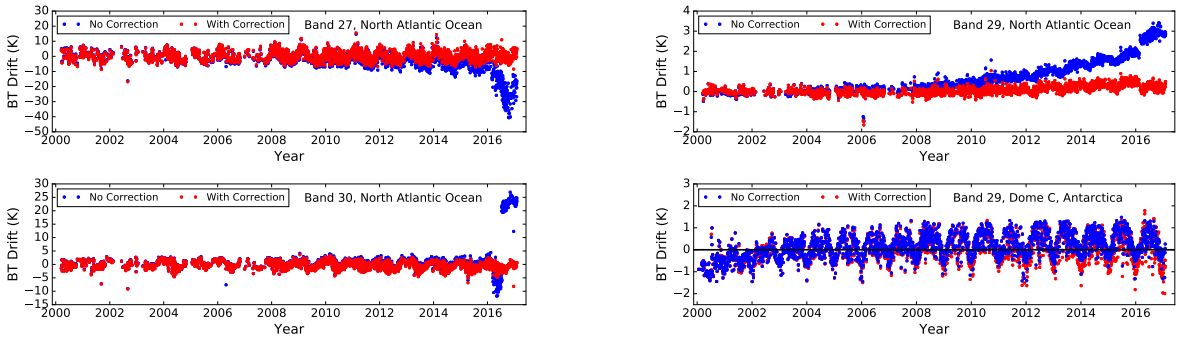

Figure 11. Examples of the brightness temperature drift relative to band 31 for selected bands and scenes. For each set of data, the drift is normalized to the averaged brightness temperature offset in 2003 for the uncorrected data. For the Dome C data for band 29, a black line is shown as a reference for the center of the oscillations in the brightness temperature drift.

Applying the crosstalk correction throughout the entire mission reduces the brightness temperature drift for each band, particularly after the safe-mode event. For band 29, the apparent discontinuity in the correction around the time of the safe-mode event appears to be mainly due to the increase in seasonal oscillations in the brightness temperature drift as the mission progressed. However, granule selection, based on our criteria for the brightness temperature of band 31 may also play a role. For the data immediately after the safe-mode, a comparison to data from the same months in 2015 before the safe-mode event show that the correction still reduces the drift of the brightness temperature relative to band 31 to nearly the same levels, even with a substantial increase in the

amount of crosstalk contamination. In late 2015 and early 2016 before the safe-mode event, the relative drift of the band 29 data appears to be approximately 0.5 K. However, after the safe-mode event, the correction reduces the drift further to approximately 0.25 K.

For band 30, the discontinuity in the uncorrected brightness temperature drift is associated with a change in the non-linear gain coefficient, a_2, for each of the detectors in band 30. The corrected data goes smoothly through this transition when the appropriate correction is applied to derive a_2, which results in the drift relative to band 31 staying near zero.

For this analysis, no data is shown for band 28, since little drift is observed in the uncorrected data. Because of this, the correction shows little difference in the average brightness temperature for these scenes relative to the variation in the brightness temperature retrieval for this band.

For the Dome C data, a measurable drift is observed in the brightness temperature relative to band 31 for band 29, as seen in the lower right plot in Figure 11. The change in the relative brightness temperature observed in the early part of the mission before 2003 is not likely due to crosstalk, since little evidence of significant crosstalk contamination is observed in band 29 in the lunar observations before this time. Also, before 2003, the detector electronics configuration was changed three times which may have a greater effect on the response for low-radiance scenes. Between 2003 and 2008, the seasonal oscillations in the brightness temperature drift are centered about the reference point, which is taken to be the average of the uncorrected data in 2003. After 2008, a slow drift is observed which clearly moves the center of the oscillations above the reference line by approximately 0.5 K. After the correction is applied, the brightness temperature drift is reduced to be centered on the reference line.

Overall, the correction to the L1B data using our derived crosstalk coefficients improves the image quality and provides an appropriate radiometric correction in order to account for the brightness temperature drift that has been observed throughout the mission.

5.1. Impact of the Correction on the MODIS Level-1B Calibrated Radiance Uncertainty

The crosstalk correction not only impacts the calibrated radiance values in the Level-1B product, but also affects the Uncertainty Index (UI), which is a measure of the radiance uncertainty on the pixel level. The algorithm for computing the uncertainty in the TEBs uses a perturbative approach, in which each input of Equation (4) is varied by the value of its associated uncertainty in order to determine how much the value of the radiance is changed for each pixel [4]. These terms are then added in quadrature in order to determine the radiance uncertainty, as seen in Equation (5).

$$\frac{\delta L_{EV}}{L_{EV}} = \sqrt{\sum_i \left(\frac{L_{EV}(x_i + \delta x_i) - L_{EV}(x_i)}{L_{EV}(x_i)} \right)^2} \tag{5}$$

After the crosstalk correction is applied, the input parameter uncertainties for some detectors can be reduced, particularly for the a_0 and a_2 gain coefficients for detectors 1, 2, 9, and 10 of band 27, and detector 8 of band 30. For the band 27 detectors, there is also a significant uncertainty reduction that is a result of a large increase in the measured radiance value after the correction is applied. In these cases, the uncertainty percentage can be lowered by as much as 20%, down to just a few percent after the safe-mode event in 2016. However, for most detectors, there is little change in the UI based on the correction when using the same method for determining the uncertainty as in [4].

For Collection 6, we also assess an additional uncertainty penalty to each of the contaminated detectors that is based on amount of remaining drift relative to band 31 after correction from our ocean data trending seen in Figure 11, which is on the order of 1% for the band average. In order to account for the time- and detector-dependence of the penalty, we assign the uncertainty penalty for each pixel according to Equation (6). This uncertainty penalty, P, is then added to the uncertainty determined using Equation (5), giving the final uncertainty value for each pixel.

$$P = \frac{\Delta dn}{dn} \beta_i \tag{6}$$

In Equation (6), Δdn is the size of the signal correction, dn is the corrected signal after background subtraction and β_i is penalty coefficient of the ith detector. The value of β is found using the ocean data trending, such that the average penalty assessed within a band matches the remaining band-averaged drift relative to band 31 after correction. For bands 28–30, the value of β is fixed for the entire band at 0.04, 0.095 and, 0.021 respectively. For band 27, β is 0.025 with detectors 1, 2, 9, and 10 having an increased value of β by 50% because of a slight offset in the corrected radiance from the rest of the band for some scenes after safe-mode (Figure 10). By making the uncertainty penalty proportional to the size of the corrected signal, Δdn, β can be constant throughout the entire mission. As the level of contamination increases, the penalty assessment increases as a result. Also, detectors with more contamination are assessed a higher penalty.

An additional assessment of the uncertainty from the derived correction coefficient values showed that this uncertainty was negligible compared to the penalty that is applied, and is therefore not included in this Collection 6 reprocessing. Overall, the uncertainty penalty introduces an additional uncertainty of 1–2% for most detectors late in the mission, with some detectors in Band 27 being assessed a 3–5% penalty for some scenes after safe-mode. Early in the mission, the uncertainty penalty is near zero for all detectors.

6. Impact on MODIS Level-2 Data

Since the crosstalk contamination among the LWIR PV bands affects the data at the earliest stages of MODIS data production, it will have a cascading impact on high level data products that rely on these bands. In particular, the MODIS Level-2 cloud product (MOD06_L2) [22] and cloud mask (MOD35_L2) [23] have been greatly affected, as both use data from the LWIR PV bands. As the mission has progressed, the crosstalk contamination has resulted in the detection of false clouds and improper cloud phase retrieval in these products. To evaluate the impact of the correction, we make comparisons of a set of threshold tests used in these products with both uncorrected and corrected Level-1B data. We compare the results of these tests to a Level-1B image from band 31, which is free from contamination and gives some indication of where we might expect to observe clouds in these tests.

The MODIS cloud mask product is used to determine the probability of clear sky for each pixel in a MODIS image. Using Level-1B calibrated radiance data from bands 1–9, 17, 18, 20–22, 26–29, 31–33, and 35, a number of tests have been developed to detect many different types of clouds. One such test uses the brightness temperature difference between bands 29 (8.6 μm) and 31 (11 μm) in order to determine the presence of ice clouds over liquid water surfaces. This test relies on the differential absorption that occurs between the two channels as the result of the presence of a cloud, which lowers the measured brightness temperature of band 31 with respect to band 29. If the brightness temperature difference between bands 29 and 31, B29–B31, is more positive than -0.5 K, then a pixel is registered to have detected ice clouds. A difference more negative than -0.5 K registers no ice cloud. Given the drift in brightness temperature induced by the crosstalk contamination as seen in Figure 11, which is greater than 2 K, and the sensitivity of this test to the band 29 brightness temperature, the applied correction will have a significant impact on the results of this test.

Figure 12 shows the results of this threshold test with and without the correction applied over an ocean scene on 1 April 2015, with an image from band 31 at 11 μm for comparison. In the band 31 image, the color scale goes from white to black with increasing brightness temperature, meaning that the brightest parts of the image represent the coldest parts of the scene and show where we would expect detection of ice clouds with the B29–B31 threshold test. In the center image of Figure 12, we show the results of the test without the crosstalk correction, where the white pixels represent the detection of ice clouds. In this image, we can see that the test detects ice clouds over a large fraction of the granule, including parts of the granule where we do not expect ice clouds. In the right image of Figure 12, we show the B29–B31 test after the crosstalk correction is applied. Here we see that the correction

significantly reduces the amount of false cloud detection, and the resulting cloud mask is much closer to what is expected based on the band 31 image.

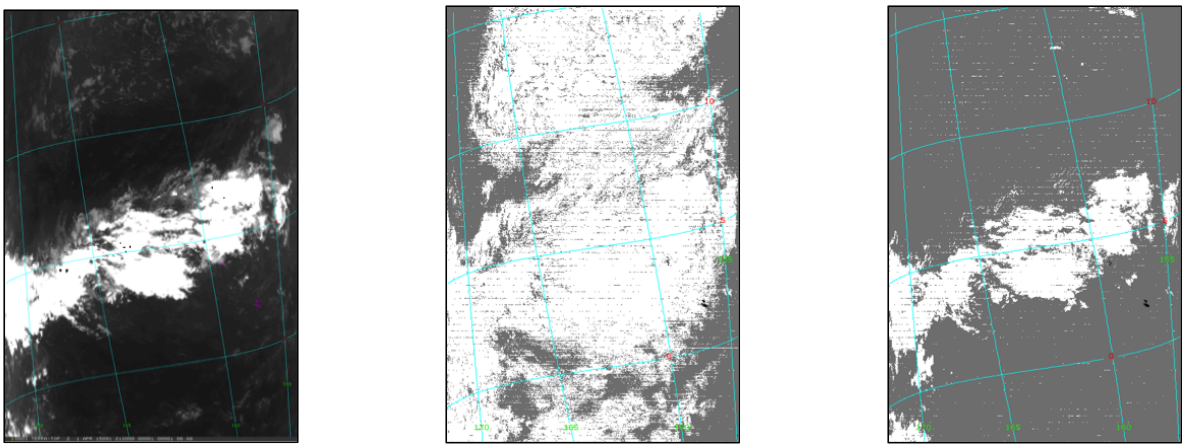

Figure 12. Terra MODIS band 31 (11 μm) imagery (**left**) on 1 April 2015, Cloud Mask ice cloud test result before crosstalk correction (**center**) and after crosstalk correction (**right**). Ice particles are indicated by cold (bright) scenes in the 11 μm imagery. Before crosstalk correction, the ice cloud test falsely detects ice clouds over the large majority of the granule, including over water clouds and clear scenes. After crosstalk correction, ice clouds are only detected in the region of the high cold clouds in the 11 μm imagery.

We also performed tests of the crosstalk correction impact on the cloud mask throughout various points in the mission and achieved similar positive results. This includes tests performed for granules after the safe-mode anomaly in February 2016, where the increase in the measured brightness temperature of band 29 due to crosstalk contamination can cause nearly entire scenes to register ice clouds without the correction. Other cloud mask tests, such as the band 27 (6.7 μm) cloud mask test for detecting thick, high-altitude clouds have also shown effects from crosstalk contamination with a similarly successful correction, although the impact of the contamination is less than the B29–B31 test [14].

Another cloud product that has been negatively impacted by crosstalk contamination is the cloud particle phase (CPP) product, which uses data from bands 28, 29, 31, and 32 to distinguish between clouds in water and ice phases. This test uses a number of logical threshold tests which compare the brightness temperature of single bands or the difference in brightness temperature of two bands. The outcome of the tests determines whether the cloud phase is retrieved as ice, water, or uncertain.

In Figure 13, we show the retrieval of the CPP for the same granule as in Figure 12 before and after correction with a band 31 reference image to the left. Before the correction is applied, the CPP retrieval shows a large amount of uncertain retrieval over the scene away from the brightest parts of the band 31 image, which should be predominately water clouds. This uncertainty in the retrieval is mainly due to an increase in the B29–B31 brightness temperature difference as a result of the crosstalk contamination, and closely resembles the false ice cloud retrieval from the cloud mask test in the middle image of Figure 12. After the correction is applied, the uncertain retrievals are reduced significantly, and warm parts of the band 31 image are then retrieved as either being clear or having water clouds as expected.

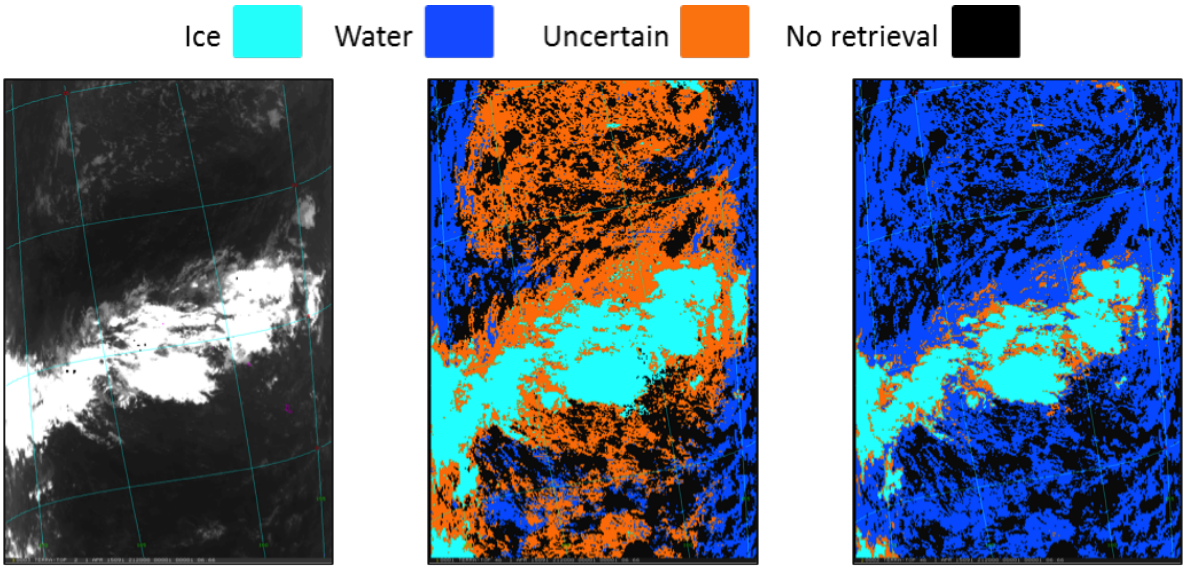

Figure 13. Terra MODIS Band 31 (11 μm) imagery (**left**) on 1 April 2015, Cloud Particle Phase product before crosstalk correction (**center**) and after crosstalk correction (**right**). Ice particles are indicated by cold (bright) scenes in the 11 μm imagery. Before crosstalk correction, the CPP data shows abundant mixed phase retrievals (orange) where data scenes are clear or contain water cloud. After crosstalk correction, these scenes are correctly retrieved as either clear or water cloud.

The crosstalk correction on the Level-2 products have been analyzed using one month of data in each year since launch. In each case, the results of these tests are consistent with the expected behavior of product, and many of the drifts associated with the increasing levels of contamination have been reduced significantly. Also, the tests show that the correction is still effective after the 2016 safe-mode event, when the contamination levels increased drastically. The impact of the correction will be continuously monitored in forward production on these products for Collection 6. Any feedback from this analysis will be used to improve the correction in future collections.

7. Conclusions

Using lunar observations, we were able to effectively characterize and derive correction coefficients for the crosstalk contamination of the LWIR PV bands in Terra MODIS. From these lunar observations, we determined that the contaminating signal included a significant component from other detectors within the same band which had not been taken into account in previous work. The correction coefficients were derived for each detector of bands 27–30 using each scheduled lunar observation throughout the entire mission. We found that these coefficients both increased steadily and had many sudden changes at various points throughout the mission. Using satellite geolocation data, we determined that these sudden changes are generally associated with a passage through the South Atlantic Anomaly, where the flux of high-energy charged particles that can damage the spacecraft electronics is relatively high.

The derived crosstalk coefficients were applied to the MODIS Level-1A data, which corrected both the detector gain parameters and the background subtracted Earth-view signal. Using the corrected Level-1A data, we were able to significantly reduce the sudden changes and drift in the detector gain parameters. With the corrected data, new Level-1B and Level-2 data products were derived for evaluation. We found that the Level-1B images showed a significant reduction in the detector-to-detector differences that resulted in the removal of striping from the images and an overall improvement in the image quality. Also, the radiometric drifts that were caused by the crosstalk contamination were significantly reduced over selected reference sites that were used for evaluation purposes. Our correction of the Level-1B data also provided an improvement in the Level-2 cloud mask

and cloud particle phase products, where false cloud detection and uncertain cloud phase retrieval were greatly reduced.

The crosstalk correction using this algorithm will be implemented in Collection 6 beginning in July 2017 for forward processing, with the full mission reprocessing beginning after the initial forward processing update. Refinements and improvements to the algorithm will be evaluated for future collections and forward processing updates if they are deemed appropriate.

Acknowledgments: The work presented here would not be possible without the dedication and efforts of many current and former members of the MODIS Characterization Support Team, who spent many years gaining insight into the nature of the crosstalk contamination for this instrument. The authors would like to acknowledge Graziela Keller, Daniel Link, and Amit Angal of MCST for their helpful comments and discussions for this work, and Na Chen of MCST for her help in producing Level-1B data for testing. The authors would also like to acknowledge Ed Masuoka, Gang Ye, and the MODAPS staff for their production of MODIS test data sets that supported the evaluation of the crosstalk correction in this paper. The authors would also like to thank Tiejun Chang and Yonghong Li for their efforts and insights into characterizing the instrument contamination in the early stages of this work using other methods.

Author Contributions: T.W. was the principle investigator for this work and took a lead role in the algorithm development and data analysis. A.W. contributed to algorithm development and to the overall analysis of Level-1B imagery. A.S. contributed to algorithm development and validation, the Level-1B data analysis over Dome C, and the uncertainty calculations. X.G. contributed to the implementation of the correction in the Level-1B products and the analysis of the impact of the correction on the Level-1B data. Z.W. contributed algorithm enhancements, including analysis of the in-band correction and the identification of the geolocation of the sudden changes in the coefficient values. C.M. and R.F. provided a comprehensive analysis of the impact of the crosstalk correction on MODIS Level-2 atmospheric products. X.X. provided support for the algorithm development and data analysis at all levels.

Conflicts of Interest: The authors declare no conflict of interest.

References

1. Barnes, W.L.; Xiong, X.; Salomonson, V.V. Status of Terra MODIS and Aqua MODIS. *Proc. IGARSS* **2002**, *2*, 970–972.
2. Salomonson, V.V.; Barnes, W.L.; Xiong, X.; Kempler, S.; Masuoka, E. An overview of Earth Observing System MODIS instrument and associated data systems performance. *Proc. IGARSS* **2002**, *2*, 1174–1176.
3. Xiong, X.; Sun, J.; Barnes, W.L.; Salomonson, V.V.; Esposito, J.; Erives, H.; Guenther, B. Multiyear on-orbit calibration and performance of Terra MODIS reflective solar bands. *IEEE Trans. Geosci. Remote Sens.* **2007**, *45*, 879.
4. Xiong, X.; Wu, A.; Wenny, B.N.; Madhavan, S.; Wang, Z.; Li, Y.; Chen, N.; Barnes, W.L.; Salomonson, V.V. Terra and Aqua MODIS thermal emissive bands on-orbit calibration and performance. *IEEE Trans. Geosci. Remote Sens.* **2015**, *53*, 5709.
5. Xiong, X.; Che, N.; Barnes, W. Terra MODIS on-orbit spatial characterization and performance. *IEEE Trans. Geosci. Remote Sens.* **2006**, *44*, 2198–2206.
6. Sun, J.; Xiong, X.; Barnes, W.; Guenther, B. MODIS reflective solar bands on-orbit lunar calibration. *IEEE Trans. Geosci. Remote Sens.* **2007**, *45*, 2383.
7. Sun, J.; Xiong, X.; Angal, A.; Chen, H.; Wu, A.; Geng, X. Time-dependent response versus scan angle for MODIS reflective solar bands. *IEEE Trans. Geosci. Remote Sens.* **2014**, *52*, 3159–3174.
8. Chen, H.; Xiong, X.; Angal, A.; Geng, X.; Wu, A. Alternative method of on-orbit response-versus-scan-angle characterization for MODIS reflective solar bands. *J. Appl. Remote Sens.* **2016**, *10*, 024004.
9. Xiong, X.; Chiang, K.; Wu, A.; Barnes, W.L.; Guenther, B.; Salomonson, V.V. Multiyear on-orbit calibration and performance of Terra MODIS thermal emissive bands. *IEEE Trans. Geosci. Remote Sens.* **2008**, *46*, 1790.
10. Sun, J.; Xiong, X.; Madhavan, S.; Wenny, B.N. Terra MODIS band 27 electronic crosstalk effect and its removal. *IEEE Trans. Geosci. Remote Sens.* **2014**, *52*, 1551–1561.
11. Sun, J.; Madhavan, S.; Xiong, X.; Wang, M. Investigation of the electronic crosstalk in Terra MODIS band 28. *IEEE Trans. Geosci. Remote Sens.* **2015**, *8*, 5722.
12. Sun, J.; Madhavan, S.; Xiong, X.; Wang, M. Long-term drift induced by the electronic crosstalk in Terra MODIS band 29. *J. Geophys. Res.-Atmos.* **2015**, *120*, 9944–9954.

13. Sun, J.; Madhavan, S.; Wang, M. Investigation and mitigation of the crosstalk effect in Terra MODIS band 30. *Remote Sens.* **2016**, *8*, 249.
14. Wilson, T.; Wu, A.; Geng, X.; Wang, Z.; Xiong, X. Analysis of the electronic crosstalk effect in Terra MODIS long-wave infrared photovoltaic bands using lunar images. *Proc. SPIE* **2016**, 10004, doi:10.1117/12.2240574.
15. Gascon, F.; Thèpaut, O.; Jung, M.; Francesconi, B.; Louis, J.; Lonjou, V.; Lafrance, B.; Massera, S.; Gaudel-Vacaresse, A.; Languille, F.; et al. Copernicus Sentinel-2 Calibration and Products Validation Status. *Preprints* **2016**, doi:10.20944/preprints201610.0078.v1.
16. Szewczyk, Z.A. Recovery and Comparison of Shortwave Radiances Measured by CERES Instruments Operating on TRRM and Terra Satellites. *Proc. SPIE* **2003**, *4882*, doi:10.1117/12.462378.
17. Miller-Ricci, E.; Rowe, J.F.; Sasselov, D.; Matthews, J.M.; Guenther, D.B.; Kuschnig, R.; Moffat, A.F.J.; Rucinski , S.M.; Walker, G.A.H.; Weiss, W.W.; et al. MOST Spacebased Photometry of the Transiting Exoplanet System HD 209458: Transit Timing to Search for Additional Planets. *Astrophys. J.* **2008**, *682*, 586–592.
18. Tonooka, H.; Iwasaki, A. Improvement of ASTER/SWIR crosstalk correction. *Proc. SPIE* **2004**, *5234*, 168–179.
19. Keller, G.R.; Wang, Z.; Wu, A.; Xiong, X. Aqua MODIS Band 24 Crosstalk Striping. *IEEE Geosci. Remote Sens. Lett.* **2017**, *14*, 475–479.
20. Sun, J.; Wang, M. Electronic Crosstalk in Aqua MODIS Long-Wave Infrared Photovoltaic Bands. *Remote Sens.* **2016**, *8*, 806.
21. Bourdarie, S.; Xapsos, M. The Near-Earth Space Radiation Environment. *IEEE Trans. Nucl. Sci.* **2008**, *55*, 1810.
22. Menzel, P.; Frey, R.; Baum, B. Cloud Top Properties and Cloud Phase Algorithm Theoretical Basis Document (MOD06, Collection 6). Available online: https://modis-atmos.gsfc.nasa.gov/_docs/MOD06-ATBD_2015_05_01.pdf (accessed on 1 May 2015).
23. Ackerman, S.; Frey, R.; Strabala, K.; Liu, Y.; Gumley, L.; Baum, B.; Menzel, P. Discriminating Clear Sky from Cloud with MODIS, Algorithm Theoretical Basis Document (MOD35, Collection 6). Available online: http://modis-atmos.gsfc.nasa.gov/_docs/MOD35_ATBD_Collection6.pdf (accessed on 1 October 2010).